



Contents lists available at ScienceDirect

Tetrahedron

journal homepage: www.elsevier.com/locate/tet

The A-D-A type small molecules with isomeric benzodithiophene cores: Synthesis and influence of isomers on photoelectronic properties

Linrui Duan^{b, c, 1}, Jianhua Chen^{a, b, 1}, Bin Liu^{a, b}, Xiangdong Wang^{a, b}, Weiguo Zhu^{a, b, *}, Renqiang Yang^{c, **}

^a School of Materials Science and Engineering, Jiangsu Collaboration Innovation Center of Photovoltaic Science and Engineering, Changzhou University, Changzhou, 213164, China

^b College of Chemistry, Key Lab of Environment-Friendly Chemistry and Application in Ministry of Education, Xiangtan University, Xiangtan, 411105, China

^c Qingdao Institute of Bioenergy and Bioprocess Technology, Chinese Academy of Sciences, Qingdao, 266101, China

ARTICLE INFO

Article history:

Received 12 October 2016

Received in revised form

12 December 2016

Accepted 19 December 2016

Available online xxx

Keywords:

Benzodithiophene

Diketopyrrolopyrrole

Isomeric small molecules

Photovoltaic performance

Organic solar cells

ABSTRACT

Two isomeric A-D-A type small molecules (SMs) of BDTx-2TVTDPP and BDTy-2TVTDPP were designed and synthesized, which contain different donor (D) center of substituted benzodithiophene (BDT) in backbone, and the same acceptor (A) and bridged units of diketopyrrolopyrrole (DPP) and thienylenevinyleneethiophene (TVT), respectively. Their thermal stability, crystallinity, film morphology and photoelectronic properties were primarily investigated. It was found the BDTx-2TVTDPP with 2,6-substituted BDT unit exhibited a pronouncedly red-shifted and enhanced absorption in solid state and a better crystallinity. In contrast, the BDTy-2TVTDPP with 4,8-substituted BDT unit in backbone exhibited better solubility, deeper HOMO energy level and more smoothed blend film morphology. As a result, the solution-processing BDTy-2TVTDPP based solar cells displayed better photovoltaic properties than the BDTx-2TVTDPP based ones using fullerene derivatives (PC₆₁BM or PC₇₁BM) as electron acceptor. A power conversion efficiency maximum of 2.85% was obtained in the BDTy-2TVTDPP based cells, which is 1.8 times that of the BDTx-2TVTDPP based cells. This study indicates that changing the substituted positions of BDT is available to significantly improve photovoltaic properties for its resulting SMs.

© 2016 Elsevier Ltd. All rights reserved.

1. Introduction

Solution-processable small molecules (SMs) have recently been made progress in bulk hetero-junction (BHJ) organic solar cells (OSCs) with a rising power conversion efficiency (PCE) of 10.01% through device optimization,¹ which is comparable to that of polymer counterparts. In order to improve cell's efficiency, numerous new photovoltaic donor materials with electron-rich donor (D) and electron-deficient acceptor (A) units have been developed in the past few years.^{2–8} With different combination of these developed D and A units, various SMs with different

molecular configurations were obtained, such as D-A-A₁,^{9–11} A-D-A,^{12–19} A₁-A-D-A-A₁,²⁰ A₁-D-A-D-A₁²¹ and D₁-A-D-A-D₁.^{22,23} It is further found that the molecular configurations have played an important role in improving photovoltaic properties for these photovoltaic SMs. For instance, the DR-3TBDTT SM with an A-D-A configuration displayed a PCE of 8.12% in OSCs.^{17–19} Another p-DTS(FBTTh₂)₂ SM with D₁-A-D-A-D₁ configuration presented an increasing PCE of 8.9%.²³

As alkyl chain and isomeric unit were found to be an important influence on the photoelectronic properties, solubility, miscibility with PCBM and active layer morphology for SMs, many works have been focused on them to tune photovoltaic performance, such as the length, the shape and the chirality of alkyl side chains,^{24–27} as well as the isomers caused by atom position^{28,29} and the linkage position of group.³⁰ The results indicate that even a subtle change in alkyl chain and isomeric unit can result in a significant difference in optical, morphological, and device properties. For example, Fréchet et al. shifted the substituted site of pyrene from C1 to C2,

* Corresponding author. School of Materials Science and Engineering, Jiangsu Collaboration Innovation Center of Photovoltaic Science and Engineering, Changzhou University, Changzhou, 213164, China.

** Corresponding author.

E-mail addresses: zhuwg18@126.com (W. Zhu), yangrq@qibebt.ac.cn (R. Yang).

¹ Both authors contribute equally to this work.

which led to an enhancement of PCE from 0.7% to 2.4% for its molecule,³¹ indicating that end-group symmetry has a dramatic influence on PCE.

Diketopyrrolopyrrole (DPP) and benzodithiophene (BDT) are common building blocks, and have been widely used to construct D-A type low band-gap polymers and SMs.^{32,33} In order to explore influence of the linked positions of the BDT central units on photoelectronic properties, herein, we designed and synthesized two A-D-A type isomeric SMs based on BDT and DPP units, namely, BDTx-2TVTDPP and BDTy-2TVTDPP. Their molecular structures are shown in Fig. 1, in which 2-ethylhexylthiophen-substituted benzodithiophene (BDTx and BDTy) with different linked positions in backbone, diketopyrrolopyrrole (DPP) and thienylenevinylene-thiophene (TVT) were used as central donor, terminal acceptor and bridged units, respectively.

The thermal stability, crystallinity, UV-vis absorption, electrochemical behavior, theoretical calculation, photovoltaic performance, carrier mobility and active layer morphology were systematically investigated. It is found that the linked positions of BDT unit have a significant impact on photovoltaic properties for both BDT-based SMs. The BDTy-2TVTDPP with 4,8-substituted BDT unit displayed better photovoltaic properties than the BDTx-2TVTDPP with 2,6-substituted BDT unit in their solar cells using fullerene derivatives (PC₆₁BM or PC₇₁BM) as electron acceptors. A power conversion efficiency maximum of 2.85% was obtained in the BDTy-2TVTDPP based cells, which is 1.8 times that of the BDTx-2TVTDPP based cells.

2. Experimental section

2.1. Materials

All reactions were conducted under an argon atmosphere. All commercial reagents were directly used without further purification. The synthetic route was shown in Scheme 1.

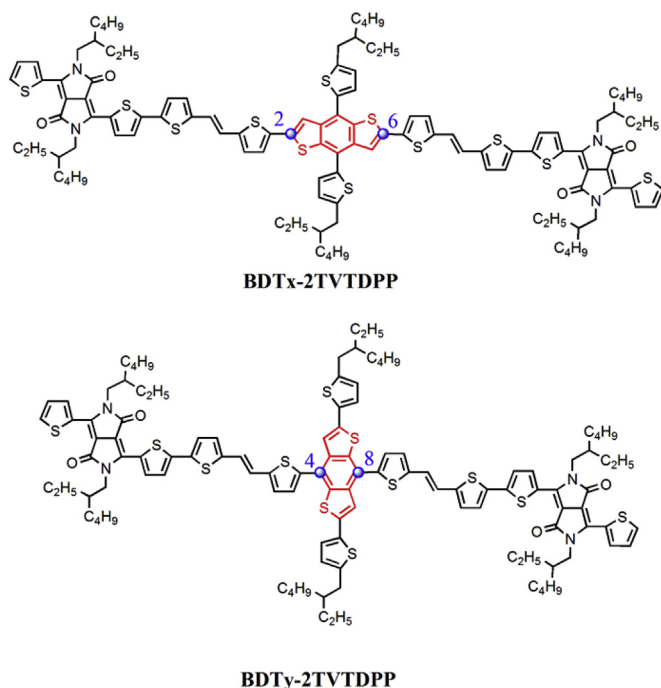


Fig. 1. The molecular structure of BDTx-2TVTDPP and BDTy-2TVTDPP.

2.2. Measurement and characterization

¹H NMR spectra were respectively recorded at 400 MHz on a Bruker Avance-400 spectrometer using CDCl₃ as the solvent and tetramethylsilane (TMS) as the internal standard unless specified otherwise. Absorption spectra were recorded on a Shimadzu UV-1800 spectrophotometer. Thermogravimetric analysis (TGA) was measured with a Perkin-Elmer Diamond TG/DTA thermal analyzer. Cyclic voltammetry was conducted on a Shanghai Chenhua CHI620 voltammetric analyzer under argon atmosphere in an anhydrous acetonitrile solution of tetra(n-butyl)ammonium hexafluorophosphate (0.1 M). A platinum dish and a platinum wire were respectively used as working electrode and counter electrode, and an Ag/AgCl electrode was used as reference electrode. SMs were coated on the surface of platinum dish and all potentials were corrected against Fc/Fc⁺. Mass spectra were measured with a Bruker Daltonics BIFLEX III MALDI-TOF analyzer using MALDI mode.

2.3. Device fabrication and characterization

All devices were fabricated on indium tin oxide (ITO)-coated glass substrates, which were cleaned by ultrason wave with detergent, deionized water, acetone, and isopropyl alcohol, respectively for 20 min. Poly(3,4-ethylenedioxythiophene)/poly(styrenesulfonate) (PEDOT:PSS, Clevis™ P Al 4083) was spin-coated onto ITO glass and then baked at 150 °C for 10 min in air. The blend solutions of SM/PC₆₁BM (or SM/PC₇₁BM) in chloroform were spin-coated onto PEDOT:PSS layer to form active layer. Ca (10 nm) and Al (100 nm) were deposited successively on active layer by thermal evaporation under high vacuum (<2 × 10⁻⁶ mbar). Current density (*J*)-voltage (*V*) curves were measured under AM1.5G illumination from a calibrated solar simulator (New-port 150 W solar simulator) with an irradiation intensity of 100 mW/cm². The external quantum efficiency (EQE) of the devices was measured on solar cell spectral response measurement system QE-R3011 (Enli Technology).

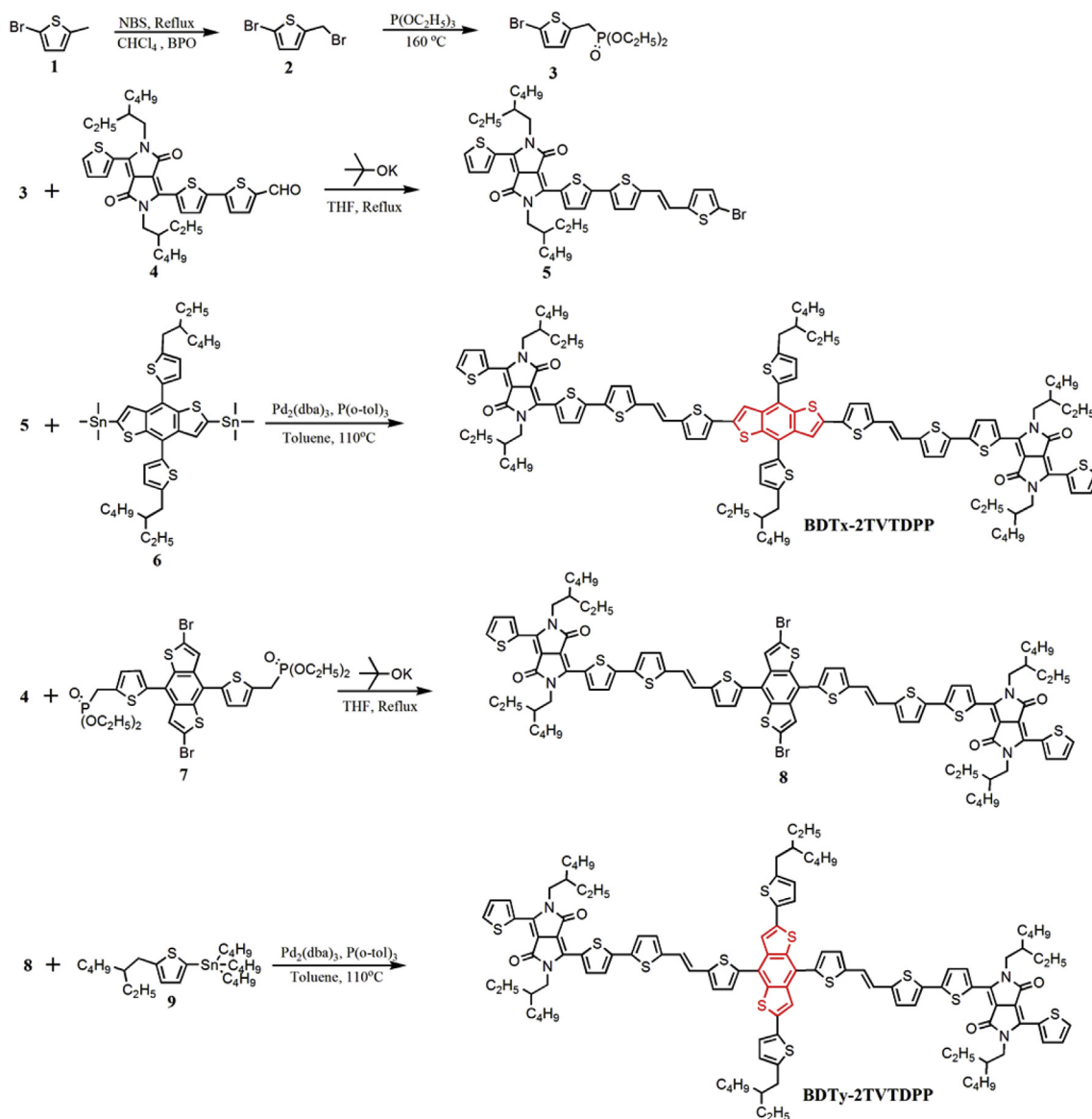
2.4. Synthesis of BDTx-2TVTDPP and BDTy-2TVTDPP

2.4.1. Synthesis of 2-bromo-5-(bromomethyl)thiophene (2)

To a solution of 2-bromo-5-methyl-thiophene **1** (5 g, 28 mmol) in tetrachloridecarbon (20 mL) were successively added NBS (12 g, 67 mmol) and benzoyl peroxide (200 mg). The reaction mixture was refluxed for 12 h under stirring. After cooled to room temperature (RT), it was filtered. The collected solution was washed with water for 3 times and dried over anhydrous MgSO₄. The organic layer was distilled to remove off the solvent and provide compound **2** as a yellow oil without any purification (5.9 g, yield 82.1%). ¹H NMR (400 MHz, CDCl₃) δ ppm, 6.88 (d, *J* = 7.0 Hz, 2H), 4.64 (s, 2H).

2.4.2. Synthesis of diethyl ((5-bromothiophen-2-yl)methyl) phosphonate (3)

Compound **2** (3.2 g, 12.5 mmol) and triethylphosphite (8 mL) were put into a 50 mL flask and stirred at 160 °C for 8 h. The excess triethylphosphite was removed off by vacuum distillation at 100 °C under 20 mmHg and the residue was purified by silica gel column chromatography using petroleum ether (PE)/acetic ether (AE) (v/v, 1:1) as eluent to obtain compound **3** as a pale yellow oil liquid (3.4 g, yield 87.2%). ¹H NMR (400 MHz, CDCl₃) δ ppm, 6.89 (d, *J* = 3.2 Hz, 2H), 6.73 (s, 2H), 4.17–4.03 (m, 4H), 3.27 (d, *J* = 20.8 Hz, 2H), 1.40–1.20 (m, 6H).



Scheme 1. Synthetic route of BDTx-2TVTDPP and BDTy-2TVTDPP.

2.4.3. Synthesis of (*E*)-3-(5'-(2-(5-bromothiophen-2-yl)vinyl)-[2,2'-bithiophen]-5-yl)-2,5-bis(2-ethyl hexyl)-6-(thiophen-2-yl)pyrrole [3,4-*c*]pyrrole-1,4(2*H*,5*H*)-dione (5)

To a solution of compound **3** (270 mg, 0.43 mmol) and compound **4** (400 mg, 0.32 mmol) in THF (10 mL), which was degassed with nitrogen atmosphere for 30 min at RT under stirring, was added dropwise another solution of potassium tertbutoxide (84 mg, 0.64 mmol) in THF (4 mL). The reaction mixture was stirred for 5 h at RT and 12 h at 60 °C successively. After cooled to RT, the resulting mixture was extracted with dichloromethane (DCM, 100 mL). The collected organic phase was dried over anhydrous MgSO₄. After the solvent was distilled off by rotary evaporation, the residue was purified by silica gel column chromatography using DCM-PE(v/v, 1:1) as eluent to give blue solid (244.6 mg, yield 49.3%). ¹H NMR (400 MHz, CDCl₃) δ ppm, 8.95 (d, *J* = 4.0 Hz, 1H), 8.90 (d, *J* = 3.4 Hz, 1H), 7.62 (d, *J* = 4.8 Hz, 1H), 7.34–7.27 (m, 2H), 7.21 (d, *J* = 3.6 Hz, 1H), 6.98 (d, *J* = 3.6 Hz, 1H), 6.96 (d, *J* = 3.2 Hz, 1H), 6.91 (d, *J* = 11.0 Hz, 2H), 6.80 (d, *J* = 3.6 Hz, 1H), 4.04 (d, *J* = 6.4 Hz, 4H), 1.89 (d, *J* = 6.8 Hz, 2H), 1.47–1.11 (m, 16H), 0.99–0.75

(m, 12H). Elementary Analysis Calculated for C₄₀H₄₅BrN₂O₂S₄; C, 60.51; H, 5.71; N, 3.53; Found: C, 60.31; H, 5.81; N, 3.62. MALDI-MS (*m/z*): 794.15; Found: 794.23 [M⁺].

2.4.4. Synthesis of BDTx-2TVTDPP

(4,8-bis(5-(2-ethylhexyl)thiophen-2-yl)benzo[1,2-*b*:4,5-*b'*]dithiophene-2,6-diyl)bis(tri-methylstannane) (67 mg, 0.074 mmol) and compound **5** (130 mg, 0.16 mmol) were dissolved in toluene (10 mL). Tris(dibenzylideneacetone)dipalladium(Pd₂(dba)₃, 20 mg) and tri-*o*-tolylphosphine (40 mg) were then added and the mixture was heated to 110 °C and stirred for 4 h. After cooled to RT, the resulting mixture was poured into 100 mL water and extracted with DCM (100 mL). The collected organic phase was dried over anhydrous MgSO₄. After the solvent was distilled off by rotary evaporation, the residue was purified by silica gel column chromatography using DCM-PE(v/v, 4:1) as eluent to give blue solid (76.4 mg, yield 51.3%). ¹H NMR (400 MHz, CDCl₃) δ ppm, 8.92 (d, *J* = 4.0 Hz, 1H), 8.84 (d, *J* = 3.6 Hz, 1H), 7.42 (d, *J* = 4.6 Hz, 1H), 7.24 (d, *J* = 4.8 Hz, 1H), 7.21 (d, *J* = 4.8 Hz, 1H), 7.11 (d, *J* = 4.6 Hz, 1H), 6.96

(d, $J = 3.8$ Hz, 2H), 6.86 (d, $J = 3.8$ Hz, 2H), 6.56 (d, $J = 3.6$ Hz, 2H), 6.41 (d, $J = 3.6$ Hz, 2H), 3.90 (b, 4H), 2.97 (d, $J = 5.4$ Hz, 2H), 1.83 (b, 3H), 1.53–1.05 (m, 24H), 0.98–0.80 (m, 18H). Elementary Analysis Calculated for $C_{114}H_{130}N_4O_4S_{12}$; C, 68.29; H, 6.54; N, 2.79; Found: C, 68.27; H, 6.58; N, 2.85. MALDI-MS (m/z): 2003.68; Found: 2003.828 [M^+].

2.4.5. Synthesis of compound **8**

To a solution of compound **4** (419 mg, 0.60 mmol) and compound **7** (244 mg, 0.30 mmol) in THF (20 mL), which was degassed with nitrogen atmosphere for 30 min at RT under stirring, was added dropwise another solution of potassium tertbutoxide (84 mg, 0.64 mmol) in THF (6 mL). The reaction mixture was stirred for 5 h at RT and 12 h at 60 °C successively. After cooled to RT, the resulting mixture was extracted with DCM (100 mL). The collected organic phase was dried over anhydrous $MgSO_4$. After the solvent was distilled off by rotary evaporation, the residue was purified by silica gel column chromatography using DCM-PE (v/v , 2:1) as eluent to give blue solid (410 mg, yield 68.6%). 1H NMR (400 MHz, $CDCl_3$) δ ppm, 8.96 (d, $J = 4.0$ Hz, 1H), 8.90 (d, $J = 3.4$ Hz, 2H), 7.67 (d, $J = 5.6$ Hz, 2H), 7.62 (d, $J = 4.7$ Hz, 2H), 7.53 (d, $J = 5.6$ Hz, 2H), 7.38 (s, 2H), 7.34 (d, $J = 4.1$ Hz, 2H), 7.23 (s, 4H), 7.14 (d, $J = 9.4$ Hz, 2H), 7.07 (d, $J = 3.6$ Hz, 2H), 4.03 (d, $J = 6.6$ Hz, 8H), 1.88 (s, 4H), 1.37–1.25 (m, 32H), 1.01–0.74 (m, 24H). Elementary Analysis Calculated for $C_{90}H_{92}Br_2N_4O_4S_{10}$; C, 60.93; H, 5.23; N, 3.16; Found: C, 60.96; H, 5.68; N, 3.18. MALDI-MS (m/z): 1773.27; Found: 1773.59 [$M + H^+$].

2.4.6. Synthesis of BDTx-2TVTDPP

Tributyl(thiophen-2-yl)stannane (**9**) (120 mg, 0.25 mmol) and compound **8** (100 mg, 0.56 mmol) were dissolved in toluene (10 mL). Tris(dibenzylideneacetone)dipalladium ($Pd_2(dba)_3$, 2 mg) and tri-*o*-tolylphosphine (4 mg) were then added and the mixture was heated to 110 °C and stirred for 4 h. After cooled to RT, the resulting mixture was poured into 50 mL water and extracted with DCM (50 mL). The collected organic phase was dried over anhydrous $MgSO_4$. After the solvent was distilled off by rotary evaporation, the residue was purified by silica gel column chromatography using DCM-PE (v/v , 4:1) as eluent to give blue solid (85.7 mg, yield 76.5%). 1H NMR (400 MHz, $CDCl_3$) δ ppm, 9.01 (d, $J = 3.9$ Hz, 2H), 8.94 (d, $J = 3.2$ Hz, 2H), 7.81 (d, $J = 5.5$ Hz, 2H), 7.66 (d, $J = 4.7$ Hz, 2H), 7.58 (d, $J = 6.0$ Hz, 4H), 7.49 (d, $J = 15.7$ Hz, 2H), 7.36 (d, $J = 3.9$ Hz, 2H), 7.28 (d, $J = 3.5$ Hz, 4H), 7.18 (d, $J = 15.7$ Hz, 2H), 7.12 (d, $J = 2.9$ Hz, 2H), 7.07 (d, $J = 3.3$ Hz, 2H), 6.91 (s, 2H), 4.20–3.98 (m, 8H), 2.94 (t, $J = 7.5$ Hz, 4H), 1.94 (d, $J = 15.2$ Hz, 2H), 1.87–1.73 (m, 4H), 1.35 (m, 48H), 1.05–0.83 (m, 36H). Elementary Analysis Calculated for $C_{114}H_{130}N_4O_4S_{12}$; C, 68.29; H, 6.54; N, 2.79; Found: C, 68.36; H, 6.46; N, 2.75. MALDI-MS (m/z): 2003.68; Found: 2004.073 [M^+].

3. Results and discussions

3.1. Synthesis of BDTx-2TVTDPP and BDTy-2TVTDPP

Scheme 1 illustrates the synthetic route of BDTx-2TVTDPP and BDTy-2TVTDPP. Compounds **2**, **3**, **4**, **7** and **9** were synthesized according to the reported literature.^{34–36} Compound **5** was obtained by the Wittig reaction between compounds **3** and **4** in a yield of 49.3%. BDTx-2TVTDPP was prepared by the Still reaction between compounds **5** and **6** in a yield of 51.3%. Compound **4** reacted with compound **7** to give compound **8**. BDTy-2TVTDPP was prepared by the Still reaction between compounds **8** and **9** in a yield of 76.5%. Both target SMs were fully characterized by 1H NMR, MALDI-MS spectra and elementary analysis.

3.2. Thermal stability and crystallinity

The thermal properties of BDTx-2TVTDPP and BDTy-2TVTDPP were investigated by thermogravimetric analysis (TGA), which were carried out under a N_2 atmosphere at a heating rate of 10 °C/min. The resulting TGA curves and their detailed data are shown in Fig. S1 and Table 1, respectively. A thermal degradation temperature (T_d) over 400 °C is observed for both SMs at 5% weight loss. Furthermore, BDTy-2TVTDPP exhibits higher thermal stability than BDTx-2TVTDPP owing to different substituted positions of BDT. In order to further study their crystallinity, both differential scanning calorimetry (DSC) and X-ray diffraction (XRD) were measured. The resulting DSC and XRD curves are depicted in Figs. 2 and 3, respectively. A single melting peak (T_m) over 209 °C for both SMs and an obvious crystallization peak (T_c) of 186 °C for BDTx-2TVTDPP are observed. Moreover, BDTx-2TVTDPP exhibits an increased T_m value by at least 50 °C in comparison to BDTy-2TVTDPP, implying that BDTx-2TVTDPP has stronger intermolecular interaction. In addition, three clearly visible diffraction peaks at 2θ values of 5.9°, 17.6° and 24.8° are observed for the BDTx-2TVTDPP neat film, which correspond to its d -spacing of 15.0, 5.1 and 3.6 Å, respectively. However, there was no diffraction peak for the BDTy-2TVTDPP neat film, indicating that BDTx-2TVTDPP has a better crystallinity than BDTy-2TVTDPP in the neat films.

3.3. Optical properties

The UV-vis absorption spectra of BDTx-2TVTDPP and BDTy-2TVTDPP in DCM solution (10^{-5} M) and thin film are shown in Fig. 4. It is found that both SMs have similar absorption spectra at the range of 300–700 nm with the maximum absorption peak (λ_{max}) around 600 nm in DCM solution. Furthermore, both SMs display a red-shift absorption spectrum in their thin films instead of in DCM solution, implying that the intermolecular interaction is enhanced in their thin films. Compared to BDTy-2TVTDPP, BDTx-2TVTDPP shows an additional peak at long wavelength of 679 nm, which can be attributed to the extent of π – π interaction. This result is agreed with the better packing of BDTx-2TVTDPP than BDTy-2TVTDPP in the neat film. The calculated optical band gaps are 1.61 eV and 1.71 eV for BDTx-2TVTDPP and BDTy-2TVTDPP based on the film absorptions, respectively (see Table 2).

3.4. Electrochemical properties

Fig. 5 shows the cyclic voltammetry (CV) plots of the BDTx-2TVTDPP and BDTy-2TVTDPP based films. The onset oxidation and reduction potentials (E_{ox}/E_{red}) of 0.78/–1.0 V for BDTx-2TVTDPP and 0.98/–1.0 V for BDTy-2TVTDPP are exhibited. As the potential of Fc/Fc^+ is 0.48 V vs $Ag/AgCl$ measured in this work and the assumed energy level of ferrocene/ferrocenium (Fc/Fc^+) is –4.8 eV below the vacuum level,³⁷ the HOMO and LUMO energy levels (E_{HOMO} and E_{LUMO}) of both SMs can be calculated according to the equation: $E_{HOMO} = -(E_{ox} + 4.32)$ eV; $E_{LUMO} = -(E_{red} + 4.32)$ eV. Table 3 lists the resulting electrochemical data. As a result, the E_{HOMO}/E_{LUMO} data of –5.1/–3.32 eV for BDTx-2TVTDPP and –5.3/–3.32 eV for BDTy-2TVTDPP are calculated. It is obviously found

Table 1
Thermal properties of BDTx-2TVTDPP and BDTy-2TVTDPP.

SMs	T_d (°C) ^a	T_m (°C)	T_c (°C)
BDTx-2TVTDPP	406	263	186
BDTy-2TVTDPP	429	209	–

^a The temperature at 5% weight-loss under nitrogen atmosphere.

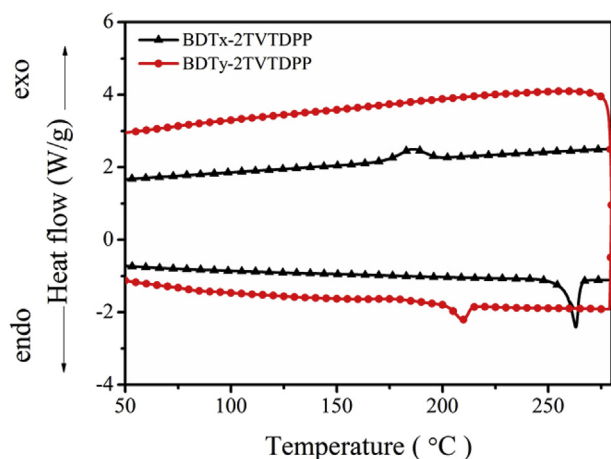


Fig. 2. DSC plots of BDTx-2TVTDPP and BDTy-2TVTDPP.

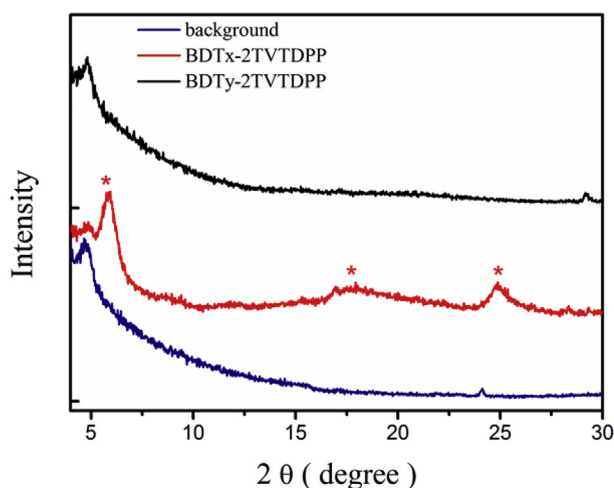


Fig. 3. XRD plots of BDTx-2TVTDPP and BDTy-2TVTDPP.

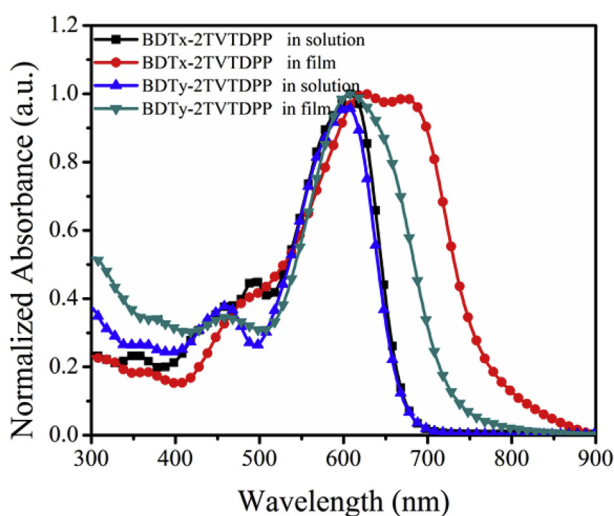


Fig. 4. UV-vis absorption spectra of BDTx-2TVTDPP and BDTy-2TVTDPP in DCM solution and their neat films.

that BDTy-2TVTDPP displays a deeper HOMO level by 0.2 eV than BDTx-2TVTDPP. Since the V_{oc} values of the photovoltaic device is

Table 2
Optical properties of BDTx-2TVTDPP and BDTy-2TVTDPP.

SMs	λ_{max} (nm) ^a	λ_{max} (nm) ^b	λ_{onset} (nm) ^b	E_g^{opt} (eV) ^c
BDTx-2TVTDPP	608	627,679	771	1.61
BDTy-2TVTDPP	605	609	726	1.71

^a The absorption in solution.

^b The absorption in thin films.

^c Calculated from the absorption band edge of the films $E_g^{opt} = 1240/\lambda_{onset}$.

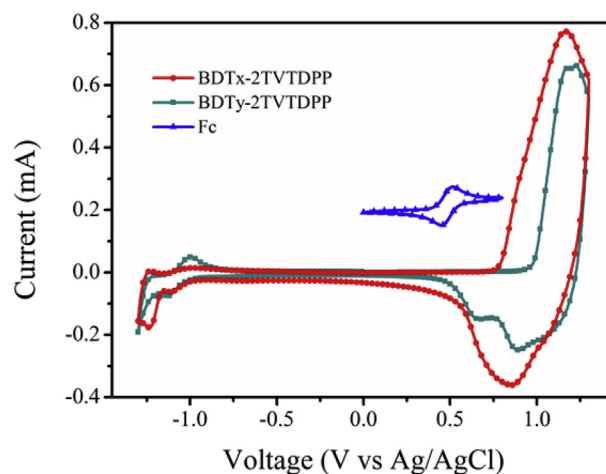


Fig. 5. Cyclic voltammogram of the BDTx-2TVTDPP and BDTy-2TVTDPP based films.

directly proportional to the energy levels offset between the HOMO of the donor and the LUMO of the acceptor,³⁸ therefore, the BDTy-2TVTDPP should possess a higher V_{oc} value than the BDTx-2TVTDPP in their solar cells.

3.5. Theoretical calculation

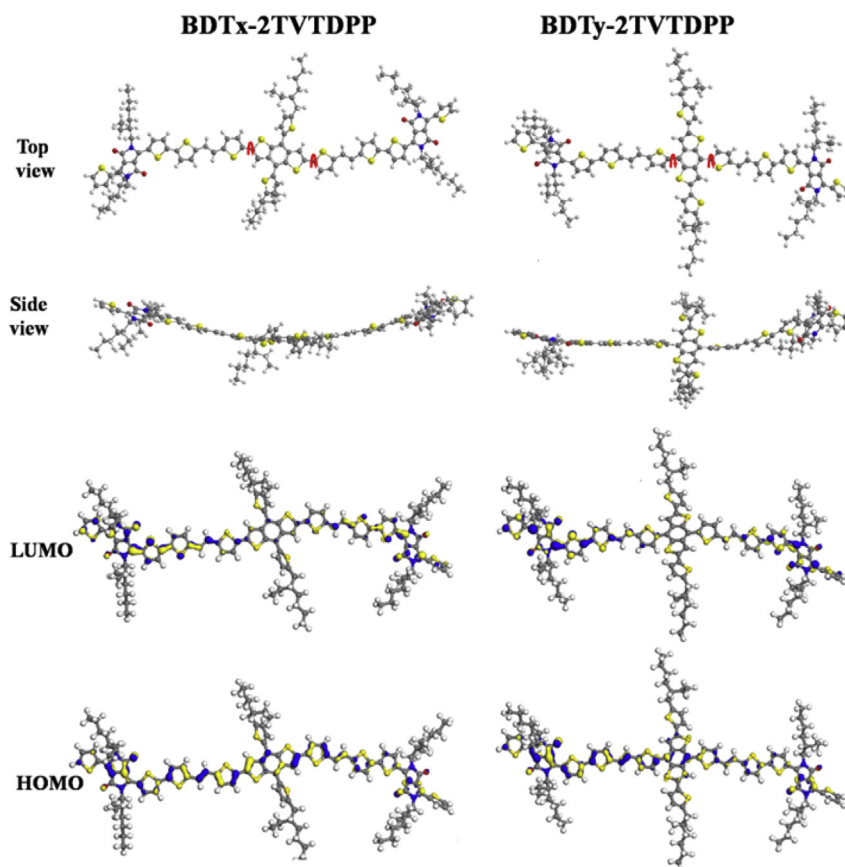
Density functional theory (DFT) calculations were performed for both SMs to get insights into their electronic structures at the B3LYP/6-31G(d) level using Gaussian 09 program. Ground state geometries are optimized at the DFT level, assuming that all thiophene rings have a *trans*-configuration in both backbone and side-chain, prior to electronic structure calculations. The optimized molecular geometries and orbital wave functions are depicted in Fig. 6. For both isomeric SMs, the HOMO wave functions are delocalized over the whole conjugated backbone. However, the LUMO wave functions are delocalized on the terminal acceptor units. It indicates that the HOMO energy levels are dominated by both donor and acceptor units, and the LUMO energy levels are governed with the terminal acceptor units, which are coincided with the electrochemical results. Moreover, the dihedral angles of $\sim 1^\circ$ and $\sim 20^\circ$ between the BDT and thienylenevinyleneethiophene moieties are observed for BDTx-2TVTDPP and BDTy-2TVTDPP, respectively. It implies that the BDTx-2TVTDPP displays better planar structure than BDTy-2TVTDPP, which result in a reduced band-gap and an increased interchain π - π interaction for BDTx-2TVTDPP as previously discussed.³⁹

3.6. Photovoltaic properties

The photovoltaic properties of BDTx-2TVTDPP and BDTy-2TVTDPP were investigated in the conventional BHJ solar devices with a structure of ITO/PEDOT:PSS(40 nm)/SM:PC₆₁BM (or PC₇₁BM)/Ca(30 nm)/Al(100 nm). The various weight ratios of the

Table 3
Electrochemical and carrier transporting properties of BDTx-2TVTDPP and BDY-2TVTDPP.

SMs	E_{ox} (V)	E_{red} (V)	E_{HOMO} (eV) ^a	E_{LUMO} (eV) ^a	E_{g}^{sc} (eV) ^b	μ_{h} (cm ² V ⁻¹ S ⁻¹)	μ_{e} (cm ² V ⁻¹ S ⁻¹)
BDTx-2TVTDPP	0.78	-1.0	-5.1	-3.32	1.78	1.61×10^{-4}	3.0×10^{-4}
BDTy-2TVTDPP	0.98	-1.0	-5.3	-3.32	1.98	2.8×10^{-5}	1.2×10^{-4}

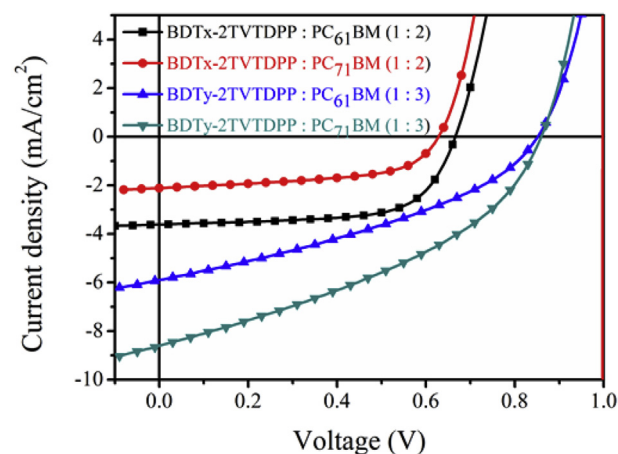
^a Calculated from empirical equation: $E_{\text{HOMO}} = -(E_{\text{ox}} + 4.32)$ eV, $E_{\text{LUMO}} = -(E_{\text{red}} + 4.32)$ eV.^b Calculated from $E_{\text{g}}^{\text{sc}} = e(E_{\text{ox}}^{\text{on}} - E_{\text{red}}^{\text{on}})$.**Fig. 6.** Molecular geometries and HOMO/LUMO wave functions of BDTx-2TVTDPP and BDY-2TVTDPP.

SM/PC₆₁BM blend films were employed from 1:1, 1:2, 1:3 to 1:4. Their photovoltaic parameters are summarized in Table 4 and the corresponding current density-voltage (*J*-*V*) curves are presented in Fig. S2 and Fig. S3. As observed, an optimized weight ratio of 1:2 for the BDTx-2TVTDPP/PC₆₁BM blend film and 1:3 for the BDY-2TVTDPP/PC₆₁BM blend film are obtained, respectively. Furthermore, BDY-2TVTDPP displays better photovoltaic properties than BDTx-2TVTDPP in their solar cells. A PCE maximum of 1.84% with a

Table 4
Photovoltaic properties of the BDTx-2TVTDPP/PCBM and BDY-2TVTDPP/PCBM based solar cells.

Donor	Acceptor	Ratio	V_{oc} (V)	J_{sc} (mA/cm ²)	FF (%)	PCE (%)
BDTx-2TVTDPP	PC ₆₁ BM	1:1	0.68	2.33	62.36	1.00
		1:2	0.67	3.61	65.82	1.58
		1:3	0.66	2.95	67.81	1.32
		1:4	0.66	2.20	65.33	0.94
	PC ₇₁ BM	1:2	0.63	2.11	56.13	0.74
BDY-2TVTDPP	PC ₆₁ BM	1:2	0.86	5.70	35.83	1.76
		1:3	0.85	5.90	36.76	1.84
	PC ₇₁ BM	1:4	0.83	5.76	37.79	1.80
		1:3	0.86	8.60	38.78	2.85

V_{oc} of 0.85 V is observed in the BDY-2TVTDPP/PC₆₁BM based cells. To further study in effect of acceptor materials on device

**Fig. 7.** *J*-*V* curves of the SM/PCBM-based solar devices under 100 mW/cm² illumination with AM 1.5 filter.

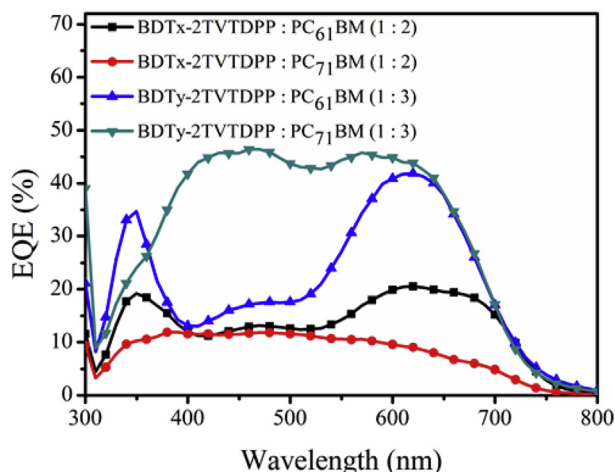


Fig. 8. EQE curves of the SM/PCBM-based solar devices.

performance, PC₇₁BM was introduced to replace PC₆₁BM because of its wider absorption region.⁴⁰ As a result, the BDTy-2TVTDPP/PC₇₁BM (1:3, w/w) based device exhibits significantly improved photovoltaic performances with increasing J_{sc} of 8.60 mA/cm² and

PCE of 2.85%. However, the BDTx-2TVTDPP/PC₇₁BM (1:2, w/w) based device shows a reverse result with decreasing photovoltaic parameters, which may be caused by its unsatisfied microcosmic nanostructures, confirmed by the blend film morphology. The photovoltaic parameters of the SM/PC₇₁BM based solar devices are also summarized in Table 4, and the J - V characteristics of the optimized SM/PC₆₁BM and SM/PC₇₁BM devices are depicted in Fig. 7. The higher V_{oc} of 0.85 V for the BDTy-2TVTDPP based cells is attributed to its lower HOMO energy level. The higher FF of 65.82% for the BDTx-2TVTDPP based cells is assigned to its better crystallinity and ordered packing.

To further understand the J_{sc} difference, the EQE curves of the optimized SM/PCBM based devices were measured as shown in Fig. 8. It is observed that all EQE curves cover a broad photoresponse wavelength range from 300 to 700 nm, which is well consistent with the absorption spectra. The BDTy-2TVTDPP/PC₇₁BM based cell displays the highest EQE value of 45%. However, the BDTx-2TVTDPP/PC₇₁BM based cells exhibit an obviously lower EQE value than the BDTx-2TVTDPP/PC₆₁BM blend. Such difference in the EQE maximum agrees well with the observed J_{sc} difference in these solar cells. The calculated J_{sc} values by integration of the EQE data for the BDTx-2TVTDPP and BDTy-2TVTDPP based devices show a ~5% mismatch in comparison with the J_{sc} values obtained from the J - V measurements.

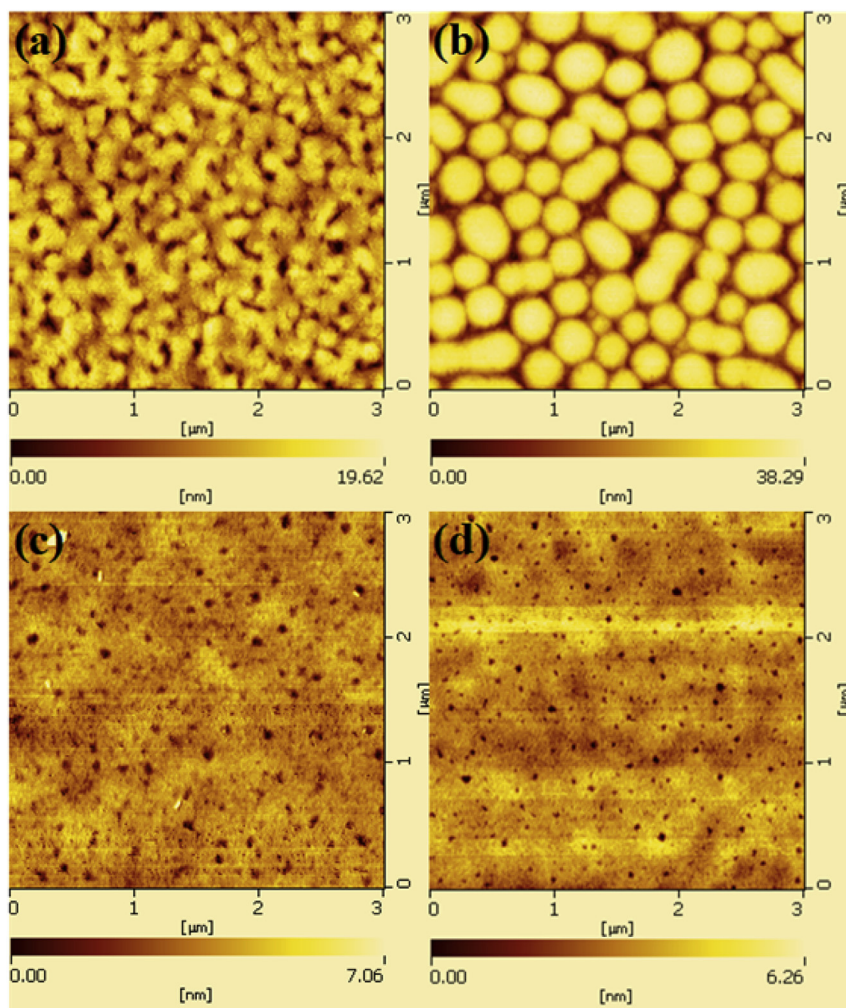


Fig. 9. AFM images for the (a) BDTx-2TVTDPP:PC₆₁BM (1:2); (b) BDTx-2TVTDPP:PC₇₁BM (1:2); (c) BDTy-2TVTDPP:PC₆₁BM (1:3); (d) BDTy-2TVTDPP:PC₇₁BM (1:3) blend films.

3.7. Mobility

The carrier mobilities of BDTx-2TVTDPP and BDTy-2TVTDPP were measured in their hole-only and electron-only devices using the space charge limited current (SCLC) method. The device structure is ITO/PEDOT:PSS/SM:PCBM/MoO₃/Al for the hole-only device and ITO/ZnO/SM:PCBM/Ca/Al for the electron-only device. Fig. S4 depicts their *J*-*V* curves in the dark. The hole and electron mobilities (μ_h and μ_e) in the BDTx-2TVT-DPP/PC₆₁BM (1:2) based devices are calculated to be 1.61×10^{-4} and 3.0×10^{-4} cm² v⁻¹ s⁻¹, which are higher than those corresponding values (2.89×10^{-5} and 1.2×10^{-4} cm² v⁻¹ s⁻¹) in the BDTy-2TVTDPP/PC₇₁BM (1:3) based devices, respectively. As a result, the corresponding μ_e/μ_h values of 1.88 for the BDTx-2TVTDPP/PC₆₁BM based devices and 4.15 for BDTy-2TVTDPP/PC₇₁BM based devices are obtained, respectively. It suggests that free charge transfer in the BDTx-2TVTDPP based device is more balanced, thus a proper FF 65.8% is obtained. In this case, the higher mobility of BDTx-2TVTDPP may be attributed to its stronger crystallinity and better ordering. Unfortunately, the BDTx-2TVT-DPP based device does not exhibit a higher *J*_{sc}. This inconsistency of *J*_{sc} with mobility may be related to its low photo-response intensity and deteriorative blend film morphology discussed below.

3.8. Film morphology

In order to further investigate difference between *J*_{sc} and mobility of the BDTx-2TVT-DPP and BDTy-2TVTDPP based devices, the morphology images of their blend films with PCBM were measured by AFM measurement, as shown in Fig. 9.

It is observed that both BDTx-2TVTDPP/PC₆₁BM and BDTy-2TVTDPP/PC₇₁BM based blend films display a large phase separation with root mean square (rms) value of 2.61 nm and 6.90 nm, respectively. By contrast, relatively smooth surface morphologies with the rms values of 0.54 and 0.55 nm are observed in the BDTy-2TVTDPP/PC₆₁BM and BDTy-2TVTDPP/PC₇₁BM based blend films, respectively, which could lead to a more efficient exciton diffusion and separation. The larger roughness of the BDTx-2TVTDPP based blend films indicates that BDTx-2TVTDPP has a higher degree of order. In addition, the domain sizes of 50 nm in the BDTx-2TVTDPP based blend films are much larger than the ideal charge diffusion length (10–20 nm). It should lead to the recombination of charge carriers, and thus the decrease of *J*_{sc} and PCE.

4. Conclusions

Two isomeric SMs of BDTx-2TVTDPP and BDTy-2TVTDPP with different substituted BDT units were obtained. The BDTx-2TVTDPP with 2, 6-substituted BDT core exhibited stronger light absorption, narrower band gap, more planar structure and better crystallinity, but worse solubility and blend film morphology than BDTy-2TVTDPP with 4, 8-substituted BDT core. In contrast, BDTy-2TVTDPP showed larger backbone torsion, better solubility, deeper HOMO energy level and smoother blend film morphology than BDTx-2TVTDPP. As a result, the BDTy-2TVTDPP based devices exhibited better photovoltaic performance than the BDTx-2TVTDPP based devices. A PCE of 2.85% was observed in the BDTy-2TVTDPP based solar cells, which is 1.8 times that in the BDTx-2TVTDPP based solar cells. The present findings highlight the importance of

the connected position of the BDT unit on improvement of photovoltaic performance for its SMs.

Acknowledgements

Thanks to the financial supports from the Major Cultivation and General Programs of the National Natural Science Foundation of China (51673031, 91233112, 21172187, 51403178, 51573154), the Program for Innovative Research Cultivation Team in University of Ministry of Education of China (1337304), the Natural Science Foundation of Hunan (2015JJ 3113), Open Project for the National Key Laboratory of Luminescent Materials and Devices (2014-skllmd-10), Research Foundation of Hunan Education Bureau (YB2015B025, 14C1099), the Hunan Postgraduate Science Foundation for Innovation (CX2014B257, CX2015B201).

Appendix A. Supplementary data

Supplementary data related to this article can be found at <http://dx.doi.org/10.1016/j.tet.2016.12.044>.

References

- Kan B, Li M, Zhang Q, et al. *J Am Chem Soc.* 2015;137:3886–3893.
- Yao H, Ye L, Zhang H, Li S, Zhang S, Hou J. *Chem Rev.* 2016;116:7397–7457.
- Hewlett RM, McLachlan MA. *Adv Mater.* 2016;28:3893–3921.
- Lu L, Zheng T, Wu Q, Schneider AM, Zhao D, Yu L. *Chem Rev.* 2015;115:12666–12731.
- Street RA, Hawks SA, Khlyabich PP, et al. *J Phys Chem C.* 2014;118:21873–21883.
- Graham KR, Cabanetos C, Jahnke JP, et al. *J Am Chem Soc.* 2014;136:9608–9618.
- Wang J, Liu K, Ma L, Zhan X. *Chem Rev.* 2016. <http://dx.doi.org/10.1021/acs.chemrev.6b00432>.
- Tang A, Zhan C, Yao J, Zhou E. *Adv Mater.* 2016. <http://dx.doi.org/10.1002/adma.201600013>.
- Qu S, Wu W, Hua J, Kong C, Long Y, Tian H. *J Phys Chem C.* 2010;114:1343–1349.
- Chiu SW, Lin LY, Lin HW, et al. *Chem Commun.* 2012;48:1857–1859.
- Lin LY, Chen YH, Huang ZY, et al. *J Am Chem Soc.* 2011;133:15822–15825.
- Loser S, Bruns CJ, Miyauchi H, et al. *J Am Chem Soc.* 2011;133:8142–8145.
- Tang W, Huang D, He C, et al. *Org Electron.* 2014;15:1155–1165.
- Ni W, Li M, Kan B, et al. *Org Electron.* 2014;15:2285–2294.
- Yong W, Zhang M, Xin X, et al. *J Mater. Chem A.* 2013;1:14214.
- Bai H, Cheng P, Wang Y, et al. *J Mater. Chem A.* 2014;2:778.
- Zhou J, Wan X, Liu Y, et al. *J Am Chem Soc.* 2012;134:16345–16351.
- Zhou J, Zuo Y, Wan X, et al. *J Am Chem Soc.* 2013;135:8484–8487.
- Kan B, Zhang Q, Li M, et al. *J Am Chem Soc.* 2014;136:15529–15532.
- Chen Y, Du Z, Chen W, et al. *Org Electron.* 2014;15:405–413.
- Wan X, Liu Y, Wang F, Zhou J, Long G, Chen Y. *Org Electron.* 2013;14:1562–1569.
- Dutta P, Yang W, Lee W-H, Kang IN, Lee S-H. *J Mater. Chem.* 2012;22:10840–10851.
- Kyaw AK, Wang DH, Wynands D, et al. *Nano Lett.* 2013;13:3796–3801.
- Lindgren LJ, Zhang F, Andersson M, et al. *Chem Mater.* 2009;21:3491–3502.
- Warnan J, Cabanetos C, El Labban A, et al. *Adv Mater.* 2014;26:4357–4362.
- Meager I, Ashraf RS, Mollinger S, et al. *J Am Chem Soc.* 2013;135:11537–11540.
- Zerdan RB, Shewmon NT, Zhu Y, et al. *Adv Funct Mater.* 2014;24:5993–6004.
- Shi J, Zhao W, Xu L, et al. *J Phys Chem C.* 2014;118:7844–7855.
- Takacs CJ, Sun Y, Welch GC, et al. *J Am Chem Soc.* 2012;134:16597–16606.
- Li S, He Z, Yu J, et al. *J Mater. Chem.* 2012;22:12523–12531.
- Lee OP, Yiu AT, Beaujuge PM, et al. *Adv Mater.* 2011;23:5359–5363.
- Lin Y, Ma L, Li Y, Liu Y, Zhu D, Zhan X. *Adv Energy Mater.* 2013;3:1166–1170.
- Huang J, Zhan C, Zhang X, et al. *ACS Appl Mater. Inter.* 2013;5:2033–2039.
- Hou J, Huo L, He C, Yang C, Li Y. *Macromolecules.* 2006;39:594–603.
- Tan H, Deng X, Yu J, et al. *Macro- Mol.* 2013;46:113–118.
- Chen J, Xiao M, Su W, et al. *Polymer.* 2014;55:4857–4864.
- Cui C, Wong W, Li Y. *Energy Environ Sci.* 2014;7:2276–2284.
- Zhou H, Yang L, You W. *Macromolecules.* 2012;45:607–632.
- Biniek L, Fall S, Chochos CL, et al. *Macromolecules.* 2010;43:9779–9786.
- Meng X, Zhao G, Xu Q, et al. *Adv Funct Mater.* 2013;24:158–163.